Three decades of coastal subsidence on the slow-moving Nice-Côte d'Azur airport area (France) revealed by InSAR : Insights into the deformation mechanism

Olivier Cavalié[1], Frédéric Cappa[2], and Béatrice Pinel-Puysségur[3]

[1]Aix-Marseille Université, CNRS, IRD, INRAE, Coll. De France, CEREGE, Aix-en-Provence, France
[2]Université Côte d'Azur, CNRS, Observatoire de la Côte d'Azur, IRD, Géoazur, Sophia Antipolis, France
[3]CEA, DAM, DIF, F-91297 Arpajon, France

Correspondence: Olivier Cavalié (cavalie@cerege.fr)

Abstract. Coastal areas can be tremendously biodiverse and host as well a substantial part of the world population and many critical infrastructures. However, there are often fragile environments that face various hazards such as flooding, coast erosion, land salinization or pollution, earthquake-induced land motions, or anthropogenic processes. In this article, we investigate the stability of the Nice-Côte d'Azur airport that has been built on reclaimed land in the Var river delta (French Riviera, France). This infrastructure has been a permanent concern since the partial collapse of the platform in 1979 and the on-going subsidence of the airport runways. Here, we used the full archive of ESA SAR images from 1992 to 2020 to comprehensively monitor the dynamics of the airport subsidence. We found that maximum downward motion rate is slowing down from 16 mm/yr in the 1990s to 8 mm/yr today. However, sediment compaction is still active and an acceleration phase of the continuous creep leading to a potential failure of a part of the platform cannot be excluded. Our study demonstrates the importance of remotely monitoring of the platform to better understand coastal land motions, which will ultimately help evaluate and reduce associated hazards.

1 Introduction

Global warming due to greenhouse gas emitted into the atmosphere is triggering a climate crisis, the impacts of which can already be felt in current times with more frequent extreme weather events such as flooding, heatwaves or wildfires. Another consequence of the global warming is the rise of the sea level, and the impact on the stability of coastal urban areas where a substantial part of the world's population lives. Actually, as the Earth's atmosphere get warmer, solid water (glaciers and ice sheets) melts and increases the quantity of sea water, that also occupies more volume because of thermal expansion (Wigley and Raper, 1987; Frederikse et al., 2020). Those two combined processes are inducing sea level rise (SLR) whose amplitude will depend on which Representative Concentration Pathway (RCP) emission scenario is followed. SLR is thus estimated for the year 2100 between 0.29 m and 0.59 m for a low emission scenario (RCP 2.6) or between 0.6 m and 1.1 m for a high emission scenario (RCP 8.5) (Oppenheimer et al., 2019). Even if the mean Earth temperature increase is kept below 2°C (compared to the pre-industrial period) within the next decades, sea level will continue to rise for several centuries or more due to the system

inertia (Schaeffer et al., 2012). This estimation is worrying as UN reports that 40% of the world population live within 100 km from the coast (more than 600 million people live in coastal areas that are less than 10 meters above sea level) and 8 of the 10 world's largest cities are near a coast.

However, sea rise is just one factor in the relative sea level changes and vertical ground motions can significantly amplify or reduce the effect of the global SLR. Indeed, sinking ground along the shoreline greatly magnifies the effects of sea level rise because both processes work together to worsen the situation (Milliman and Haq, 1996; Wöppelmann and Marcos, 2016; Wu et al., 2022). Indeed, uplift or subsidence along the coast are generated either by natural phenomena (sediment compaction (Cahoon et al., 1995), global isostatic adjustment (Farrell and Clark, 1976; Kendall et al., 2005; Peltier, 2004), or tectonics (Atwater, 1987)) or by human activities (ground water (Galloway and Burbey, 2011) or hydrocarbon extraction (Métois et al., 2020), or land reclamation (Cavalié et al., 2015)). This last one becomes more and more frequent due to population growth in coastal areas. Subsidence due to human activities are often very localized and difficult to model. They are thus often not very well known and the underlying processes remain unclear. One of the most effective method to reveal them is to measure the Earth surface displacements by InSAR (Bürgmann et al., 2000; Cavalié and Trouvé, 2022). Actually, the spatial sampling of the radar allows to map finely the location and the amplitude of these surface deformations. ~~And~~ And the more InSAR studies, the more coastal subsidence are revealed (Wu et al., 2022).

In the last few years, several studies on deformation measurements by InSAR over reclaimed lands have been published, showing the raising attention of the community for this subject. For example, Xiong et al. (2022) and Li et al. (2022) used Sentinel-1 data, covering five years, to observe subsidence over several reclaimed lands in China. Other studies processed several datasets from different sensors in order to cover a longer observation period. However, due to the lifespan of the different SAR sensors, these datasets do not overlap in time and have temporal gaps. For example, the subsidence of Urayasu city (Japan) has been measured thanks to ERS-1/2 (1993-2006), ALOS (2006-2010) and ALOS-2 (2014-2017) InSAR time series (Aimaiti et al., 2018), leading to a gap between 2010 and 2014. In this case, the temporal profile of the deformation was too irregular to enable any modelling that could connect the measurements across the temporal gap. However, in two other studies, the temporal profile of deformation was regular enough to be modelled and thus to recover a deformation spanning the whole observation timelapse: on the one hand, Park and Hong (2021) used a hyperbolic model to connect two InSAR time series measured by ALOS (2007-2012) and Sentinel-1 (2014-2019) on Busan reclaimed lands (South Korea); on the other hand, a settlement model (Plant et al., 1998) established during the preparation of Hong Kong International Airport was used to connect time series acquired over this site by ERS-2 (1998-2000), ~~ENVISAT~~ Envisat ASAR (2003-2010), Cosmo-SkyMed (2013-2017) and Sentinel-1 (2015-2018) (Wu et al., 2020). Several models for subsidence measurements are compared in Xiong et al. (2022), namely hyperbolic, Poisson and exponential models. However, in all the precited studies, the deformation modelling is limited to a mathematical function fit without a theoretical mechanical framework and real physical parameters for soils and rocks.

In this study, we process 28 years of SAR data to obtain high-quality surface deformation time series covering the Nice Côte d'Azur airport (NCA), located in the French Riviera (southeastern France) (Figure 1a). This critical economical infrastructure (it hosted 14.485 million passengers in 2019 before the pandemic) was built in the late seventies on reclaim lands over a narrow

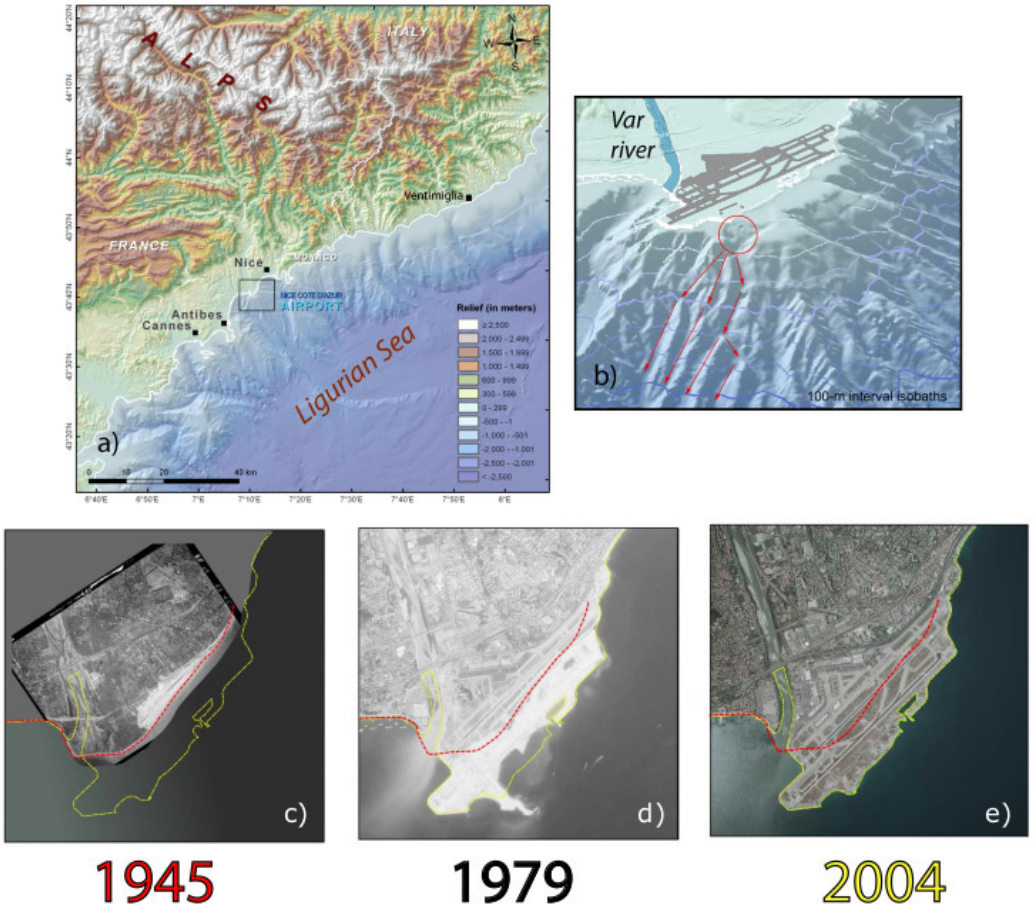

Figure 1. (a) Topographic map of the French Riviera showing the large gradient between the southern Alps and the offshore margin of the Ligurian sea (more than 4000 m elevation drop over 40 km). The black square indicates the close-up footprint shown in (b). (b) Zoom on the Nice Côte d'Azur airport with a 3-D perspective. The red circle shows the airport extension area which collapsed in 1979. The paths of the landslide are indicated with red arrows. (c-e) Three aerial photographs showing the evolution of Nice airport from the first tar runway in 1945, the maximum extension of the platform including the dyke that collapsed in October 1979, and the final shape of the airport in 2004 (it has not changed since then). On each photograph, the red and yellow dashed lines represent the coastline as it was in 1945 and 2004, respectively. (Photo credit: aerial photographies are archived by IGN and can be found at https://remonterletemps.ign.fr)

coastal shelf (1-2 km wide). Tragically, in October 1979, during the building phase, part of the airport extension collapsed in the sea, triggering a local tsunami that caused the death of 11 people (Figure 1b). Then, part of the project was cancelled (mainly the construction of a commercial port attached to the airport) but the airport platform, which had already been completed, was used to build the two main runways that are currently in use (Figure 1e).

Cavalié et al. (2015) published a first study showing that between 2003 and 2011 (the acquisition period of Envisat) the Var river delta as well as the airport that is located at its mouth, is subsiding. The spatial extent of this subsidence is strictly limited to the quaternary alluvium deposits of the delta and Var riverbed (Figure 4 in Cavalié et al. (2015)). Actually, on both sides of the riverbed, the subsidence rate quickly drops to zero where the transition from alluvium to conglomerate occurs. Moreover, the downward displacement rate increases toward the sea as the sediment layers get thicker and more recent (Figure 6 in Cavalié et al. (2015)). Indeed, it ranges from less than 1 mm/yr in the Var valley to a maximum rate of 10 mm/yr on the airport platform where sediments got brought in the 1970s to built the runways.

During the 2003-2011 period, InSAR data show essentially a steady subsidence. Here, we extended the time series in order to observe the behaviour of the airport platform over a longer period (1992-2020). ~~This long observation period provides an opportunity to investigate new mechanisms driving vertical land motion in coastal areas~~**This long observation period provides an opportunity to investigate new mechanisms driving vertical land motion in coastal areas**. Actually, no physical process could explain a constant subsidence rate over several years. We thus processed the data from the ERS satellites between 1992 and 2001 and the data acquired by Sentinel-1 for the period 2014 - 2020. Then we discussed and modelled the information brought by these new data sets. In particular, we investigated if a model of creep compaction of the airport platform can explain the data. ~~Unlike precedent studies, this model is not a simple mathematical function fit but it also includes a geomechanical framework for slow creep and the estimate of physical parameters of the slope materials.~~ **Unlike precedent studies, this model is not a simple mathematical function fit, but it uses a geomechanical framework for slow creep to estimate the physical parameters of the slope materials.** Through our investigations, we measured a deceleration of the maximum subsidence rates of the platform from 16 mm/yr (1992-2001), then 9.5 mm/yr (2003-2011) to 8 mm/yr (2014-2020) over the study area. ~~The uncertainty on subsidence rates has been carefully estimated by two different methods, both leading to estimates of about 0.3 mm/yr for the three periods, more than an order of magnitude below the measured rates.~~ **The uncertainty on subsidence rates has been carefully estimated by two different methods, both leading to estimates of about 0.3 mm/yr for the three periods, more than an order of magnitude below the measured rates.** We find that the non-linear surface displacement can be explained by a transient creep mechanism that fits the whole temporal evolution of observations. These results are useful for future physics-based forecasting models of the coastal slope evolution.

In the following sections, we shortly relate the NCA airport history. Then, we present the InSAR measurement of the airport platform deformation, including a noise analysis of the generated data set. ~~This latest point is rarely discussed in the subsidence studies, although it is crucial to accurately assess the hazard due to the subsiding area~~**This latest point is rarely discussed in the subsidence studies, although it is crucial to accurately assess the hazard due to the subsiding area**. Finally, we model the InSAR observation to better understand the underlying physical process of the platform subsidence and discuss the potential consequences of such vertical displacements.

2 History of the Airport construction

For the first half of the 20th century, Nice only hosted an aerodrome made of a single dirt track. Nice airport history really started in 1944 when the allies and the Americans set up a logistics base in Nice and thus built the first tar runway (Figure 1c). In the following years, few limited inland extensions (several hectares) of the airport platform have been done to welcome bigger planes. However, the airport is stuck between the sea and Nice city that prevents any development inland. As air traffic increased, it has been decided to extend the airport southward, on reclaimed land over sea in order to build a second runway. More than hundred of studies have been done as it is a real challenge to build there, notably because the continental shelf is very narrow (less than 2 km wide) and is bounded by very steep and deep slopes. The structural work of the platform was performed between 1975 and 1978 when 30 000 000 tons of material were brought from a neighbouring hill (Ollié, 1982). The sediments were then dynamically compacted (with a 130 kg mass falling from 23 m high). Meanwhile a 3-km long seawall have been built to protect the platform from the sea storms. In July 1978, the structural work of the airport platform was finished while construction work continued to build a dyke where a commercial port would take place. Unfortunately, the 16th of October 1979, an undersea landslide triggered the collapse of this dyke (Figure 1b,d,e). As a result, the port project got dropped, and the next three years were dedicated to consolidate the airport platform. In 1982, the last stage of the work including the construction of the pavement was achieved. The Nice airport was then inaugurated in 1983 (de la Tullaye , 1989). Since then, only minor changes were added and Figure 1e shows the shape of the airport platform as it is today.

3 InSAR measurement of the NCA airport subsidence

3.1 Data and Method

In order to extend the temporal observation window of Cavalié et al. (2015) (that spans the period 2003-2011), we processed data acquired previously by the satellites ERS and recent data acquired by the ongoing Sentinel-1 mission. The 2015 study gives important information about the deformation detected on the airport platform. In particular, it shows that the displacement is almost purely vertical (i.e., no horizontal motion stands out of the noise). So, as it is a one-dimension motion, one can process only one track and then project the line of sight (LOS) InSAR displacement into the vertical direction ~~.~~($D_{\mathrm{vert}} = D_{\mathrm{LOS}}/\cos\alpha$, **where D_{vert} is the vertical displacement, D_{LOS} the line of sight displacement, and α the incidence angle at each pixel location).** For the ERS mission, the European Space Agency (ESA) clearly favored acquisitions on descending orbits for this area. We, thus, selected the track 22 where 65 images were acquired between November 1992 and September 2001 (while only 26 images are available for the ascending track over the same period). Envisat data have been already processed in Cavalié et al. (2015). For Sentinel-1 data, we processed the descending track 139. We took advantage that Sentinel-1 SAR images are made of multiple bursts to select only those that cover the airport. As the airport is a kilometric object, only 2 bursts of the first sub-swath need to be processed.

We mostly followed the same methodology as in Cavalié et al. (2015). Ground displacement time series are generated from interferograms using the NSBAS processing chain (Doin et al., 2012). As all small baseline processing chains, the main

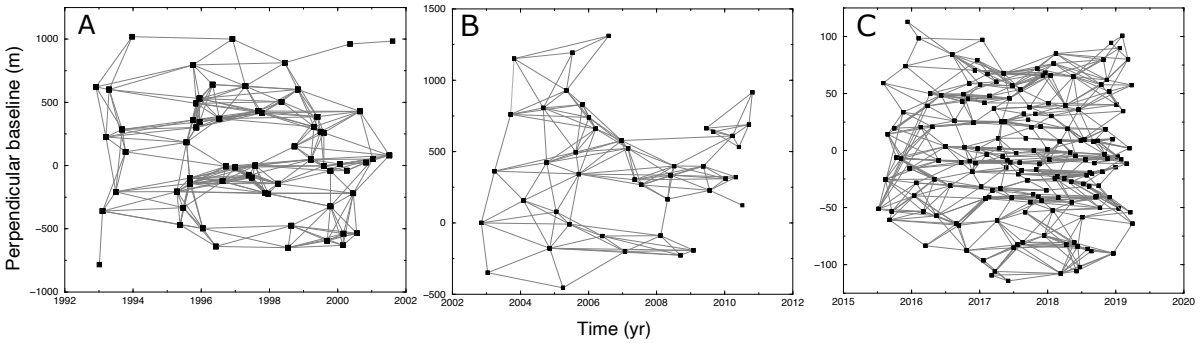

Figure 2. Relative position of orbits plotted as a function of image acquisition date for (A) descending ERS track 22, (B) descending Envisat track 22 and (C) descending Sentinel-1 track 139. Grey lines show image pairs processed into interferograms that are included in the time series analysis.

idea consists in limiting both the temporal and spatial baseline between the images that will be combined to compute the interferograms in order to optimize the interferometric phase coherence and thus keep the highest possible number of pixels for the deformation analysis. Figure 2 shows the network of interferograms based on the image acquisition configuration for ERS, Envisat, and Sentinel-1 data. However, for ERS data, this strategy was not sufficient to reduce phase noise and we used MuLSAR software (Pinel-Puysségur et al., 2012) in order to further improve the phase stability. The principle of this software is to combine different redundant paths between acquisition dates in order to reduce the phase noise level on the wrapped interferograms. **In the case of ERS data, as many interferograms are very noisy, it is necessary to filter the wrapped interferograms with a dedicated filter. Indeed, the unwrapping of interferograms is a very tricky step and large parts of interferograms may be lost if they are not properly filtered before unwrapping. Thus, the MuLSAR filter which proved efficient for the filtering of very noisy interferograms (Grandin et al., 2012) has been applied.**

ERS and Envisat interferograms are corrected for orbital and topographic components using DORIS and the ALOS DEM, respectively. ALOS DEM is also used to correct Sentinel-1 interferograms. To help the phase unwrapping, interferograms are filtered and slightly downsampled by pixel multilooking with 2 looks in range and 2×5 looks in azimuth for ERS and Envisat interferograms and 2 looks in azimuth and 2×4 looks in range for Sentinel-1 data. The resulting pixel spacing is ~ 40 m $\times$ 40 m. Interferograms are properly referenced using areas around the airport that has been proven to be stable (Cavalié et al., 2015). Finally, we used a constrained least-square inversion (Doin et al., 2012) in order to derive the surface displacement rates from the interferograms. A temporal smoothing operator is applied to limit phase variations due to turbulent atmospheric delays (although atmospheric delays are limited as InSAR is a relative measurement and we work at small scale). Surface velocity maps shown in Figure 3 are derived from the linear component of the time series for each pixel.

3.2 Surface displacements observed from 1992 to 2020

Figures 3a-c shows the averaged vertical ground velocity for the ERS (1992-2001), Envisat (2003-2011) and Sentinel-1 (2014-2020) periods. Note that the color scale changes to match the maximum velocity value. This representation allows to see that the spatial displacement pattern is steady through the whole observation window, although the amplitude decreases in time. This is a major update compared to the 2015's study (Cavalié et al., 2015) where the time window was too short to measure reliably any slow down of the surface displacement. Thus, with this new dataset, we have the opportunity to measure subsidence rate variations over a 28 year long period of time.

To better observe the temporal variations of the airport platform subsidence, Figure 3d shows the displacement evolution of pixel P_1 that is located in the maximum subsidence area (Figure 3a). As the changes of the carrier frequency between each generation of satellites prohibit cross-interferogram (Envisat-Sentinel-1 for instance), the time series is discontinued. Thus, Figure 3d shows the three trends for each satellite period (red dots). A simple linear regression reveals that, for P_1, subsidence rates were in average 16 mm/yr, 9.5 mm/yr and 8 mm/yr for the periods 1992-2001, 2003-2011, and 2014-2020, respectively. We thus observe a deceleration of 50% of the subsidence rates over 28 years. To better visualize the evolution of the pixel displacement through the full period, one can make the assumption that no sharp motion took place between the 3 measured periods and that the shape of the motion follows a logarithmic function (with Heaviside step functions to take into account the discontinuities) :

$$f(t) = a \log\left(1 + \frac{t}{b}\right) + cH_1 + dH_2 + e \quad (1)$$

where t is the time, H_1 and H_2 are two Heaviside step functions, and a, b, c, d, and e are some constants. By inversion, one can determine them and thus reconstruct the time series (Figure 3d).

3.3 Noise Analysis and Discussion

Our InSAR processing strategy turns out to be very effective and shows very nice results both in time (Figure 3d) and spatially (Figures 3a,b,c). Actually, on maps, land subsidence is clearly localised in the riverbed (we are able to detect velocity slower than 1 mm/yr) and then over the airport platform where the downward velocity increases. Qualitatively, we observe little noise in the data and unlike many studies about subsidence, we don't see any areas with artificial uplift due to atmospheric delays. Indeed, velocity drops sharply to 0 over the consolidated conglomerate located on each side of the riverbed. However, it is important to quantify the error bars on the data as it is often an important parameter for modelling the deformation.

Estimating the noise level is both very important and tricky in InSAR and thus it is often either ignored in the published InSAR studies or theoretical values are given. ~~However, several~~ **Moreover, in several studies, the noise level is estimated only on displacement measurements by computing the Root Mean Square Error between measured and modelled displacements. Even if the measurement of interest is actually velocity, uncertainty on this physical quantity is not derived (Li et al., 2022; Park and Hong, 2021; Xiong et al., 2022). In this study, uncertainties on deformation velocity are computed by two different methods and give similar estimates**.

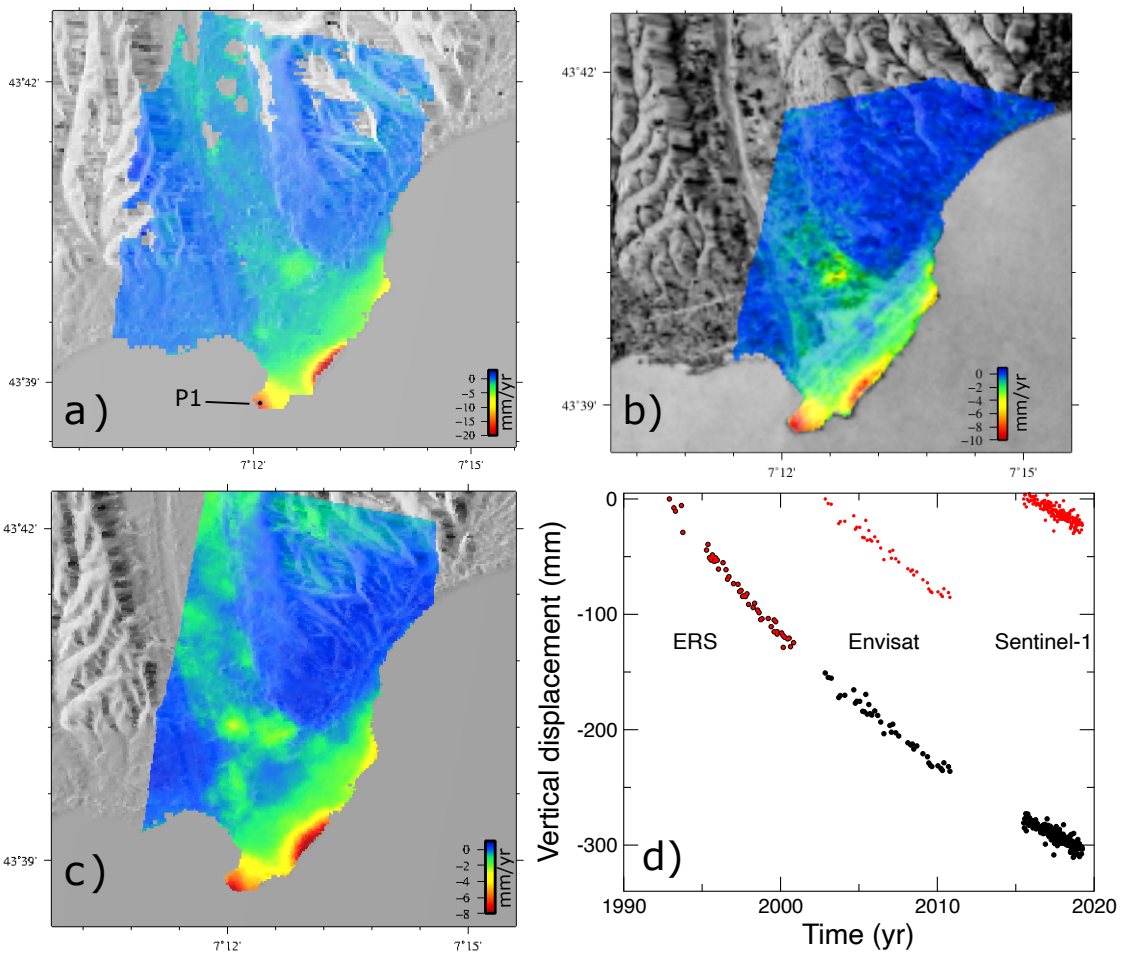

Figure 3. Projected vertical ground velocity (mm/yr~~, downward positive~~) measured from (a) ERS (1992-2001), (b) Envisat (2003-2011), and (c) Sentinel-1 (2015-2020) data. Note that the color scale changes and is adapted to show the persistent patterns of deformation over time. Black dot in (a) shows the location of pixel P1. (d) Time series of P1 vertical displacement. Red dots correspond to the three times series computed independently. Black circles represent the reconstructed time series by constraining the displacement as a logarithmic function.

Several methods have been developed to estimate the noise correlation, notably to compute the InSAR data covariance matrix that are used in the inversion to retrieve parameters of the underlying geophysical phenomena (Sudhaus and Sigurjón, 2009). In the previous study (Cavalié et al., 2015), authors evaluated the uncertainties of the velocity maps by looking at the dispersion of surface velocity measurements in a nearby location where no surface displacement is expected. As a result, all velocity variations observed in the InSAR data are due to noise. Assuming that the noise level is similar on the nearby deformed area, a 1-σ error can be computed. With this method, Cavalié et al. (2015) estimated a 1-σ error of 0.25 mm/yr for the mean subsidence rate occurred between 2003 and 2011. Similarly, using the time series, one can estimate the temporal dispersion of a pixel located on a stable area. Moreover, if the temporal evolution of the surface displacement is simple enough (as it is the case for the NCA airport), one can remove a deformation model and then observe the residue dispersion. The advantage is that the 1-σ error is computed directly in the subsiding area (and not for a pixel located nearby that can be affected by other local sources of noise). Figure 4 displays the InSAR signal residue (after removing the logarithmic function estimated from Equation 1) for the pixel P_1 (shown on Figure 3a). Overall standard deviation on displacement σ_d is ~4.2 mm. Interestingly, we see that data dispersion is very similar for the ERS, Envisat and Sentinel-1 time series (that have been processed independently). As in Fattahi and Amelung (2015), if we assume that the residue is a Gaussian white noise, the uncertainty on the deformation velocity σ_v can be estimated for each time series as:

$$\sigma_v = \frac{\sigma_d}{\sqrt{\sum_{i=1}^{N}(t_i - \bar{t})^2}} \tag{2}$$

where t_i are the acquisition dates, $\bar{t}$ is the mean acquisition date and N the number of acquisitions. σ_v is estimated to 0.27 mm/yr for ERS, 0.28 mm/yr for Envisat and 0.32 mm/yr for Sentinel-1 dataset. Interestingly, the estimate for Envisat dataset is very close to the 1-σ above mentioned error of 0.25 mm/yr estimated by a different method. Deformation velocity derived by InSAR using SBAS type techniques (Berardino et al., 2002) may be biased due to phase misclosure (De Zan et al., 2015). Recent studies suggest that this phenomenon is due to the temporal change of scattering mechanism (Ansari et al., 2021): it occurs either on vegetated areas where the scatterers vary in time due to growth or decay of the vegetation and also on bare soils where moisture level changes according to precipitation events. However, our study is focused on an urbanized area that should not be prone to this bias.

4 Creep Modelling

4.1 Geological, Hydrogeological and Geomechanical Context

The time series of surface displacement data estimated from InSAR analysis shows a non-linear transient evolution over 28 years (1992 to 2020) (Figure 3d). This reflects a progressive and long-term deformation of the sub-surface layers. Actually, soils and rocks can exhibit creep behavior, which is the development of time-dependent strains at a state of constant effective stress (Bland, 1960; Findley et al., 1976; Jaeger and Cook, 1979). Creep behavior influences the long-term stability of grounds and movement of slopes. This time-dependent material behavior exhibits viscoelastic or viscoplastic characteristics that can

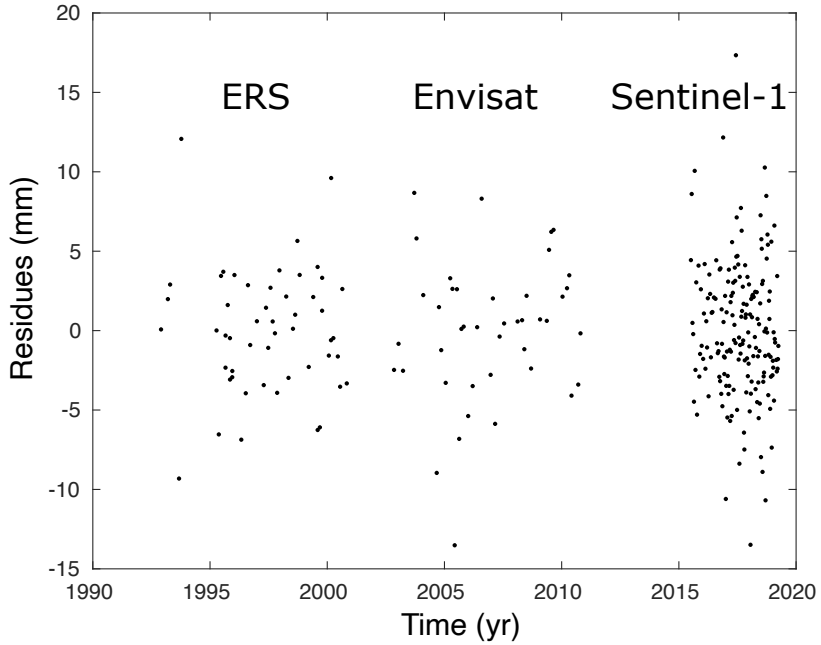

Figure 4. Displacement residues for P_1 (InSAR times series minus the fit function estimated with equation 1). Residue dispersion is $\sim$4.2 mm.

be reproduced with different creep models of increasing complexity depending on the type of material and loading conditions (Jaeger and Cook, 1979).

Previous studies of the submarine slope stability in the area of the Nice airport indicated that the geological formations below the airport deform with a slow creep process (Dan et al., 2007; Stegmann et al., 2011). Since the 1979 major landslide, an increasing collection of geological, geomechanical and geophysical data has been acquired in this area prone to failure (Kopf et al., 2016; Sultan et al., 2020) . Rohmer et al. (2020) showed that the sediment thickness is more than 100 m under the airport area. Based on a combination of field geological observations, boreholes data collected down to 100 m depth, and geophysical imaging, a number of studies have characterized the sedimentary system with (1) a basal Jurassic karstic limestones overcomed by (2) Pliocene deltaic conglomerates, (3) Early Pleistocene marls, and then covered at top by (4) a series of Holocene alluvium composed of silty and clayey lenses, sand and gravels (Stegmann et al., 2011; Sultan et al., 2020; Courboulex et al., 2020). This succession of sedimentary layers constitutes three overlapping aquifers with different permeabilities and fluid pathways (Du et al., 2019; Sultan et al., 2020). In this hydrogelogical system, pore pressure fluctuations (few tens of kPa) are sensitive to long smooth seasonal variations (Sultan et al., 2020). Importantly, a clay layer is suspected to be the creeping section of the continental slope below the sea level and a potential contributor to the origin of submarine landslide (Leynaud and Sultan, 2010; Sultan et al., 2020). This weak clay layer, situated between 30 and 45 m below the sea level, was detected from in-situ piezocone measurements (i.e., CPTU: Cone Penetration Testing) and sediment cores (Dan et al., 2007). The softening of this

sensitive layer may affect the global strength of the sedimentary system below the airport area. Consequently, it is important to investigate the creep process to explain the slope deformation and failure. In addition, the time series of surface displacement measured from 1992 to 2020 indicates that the displacement is mainly vertical and the horizontal component is negligible. This behavior suggests that a creep compaction is probably at play.

4.2 Modelling of Long-Term Slow Creep Processes

Several models have been developed to describe creep and failure in rocks (Jaeger and Cook, 1979). Creep represents strain increase with time. A typical creep curve indicates three different regions: the primary, secondary and tertiary creep region (Figure 5a). Once the material experiences an instantaneous strain, as a result of sudden loading, the primary creep region begins and has a decreasing strain rate with time. This behavior continues until the secondary stage starts with a constant strain rate. The strain rate in secondary stage is the minimum strain rate of a creep deformation. The last stage of creep deformation is the tertiary creep regime characterized by very high strain rate and eventually failure.

The shape of the observed displacement at the surface of the airport is similar to the shape of the primary and secondary creep stages of the theoretical creep curve. A viscoelastic Burger's model can effectively reflect the primary and secondary creep stages of rock creep process; however, it cannot describe the acceleration phase of tertiary creep. Here, we use an extended Burger's creep model made up of a series of Maxwell and Kelvin bodies (Jiang and Wang, 2022) to reproduce the InSAR observations. Such viscoelastic model was previously employed to model soil deformation (Yao et al., 2021), fault relaxation after earthquakes (Sun and Wang, 2015), landslide creep (Zou et al., 2013; Liao et al., 2022), and is often used in geology to illustrate the effects of both strain and stress relaxation. The transient creep (δ) with time (t) is analytically calculated as follows:

$$\delta(t) = \sigma_0 \left[\frac{1}{E_M} + \frac{t}{\eta_M} + \frac{1}{E_{K_1}} \left(1 - \exp\left(-\frac{E_{K_1} t}{\eta_{K_1}} \right) \right) + \frac{1}{E_{K_2}} \left(1 - \exp\left(-\frac{E_{K_2} t}{\eta_{K_2}} \right) \right) \right] \tag{3}$$

where E_M, E_{K_1}, E_{K_2} are the elastic moduli of the Maxwell body, the first and second Kelvin bodies, respectively; η_M, η_{K_1}, η_{K_2} are the viscosity of the Maxwell body, the first and second Kelvin bodies, respectively; σ_0 is a constant uniaxial load. The transient Kelvin component of the rheology is considered to be dominant at short timescales, while the Maxwell component dominates at long timescales (Jaeger and Cook, 1979). With this 1D model, 7 parameters need to be adjusted. We used an adaptive grid search method to invert the parameters. We set up the search range of each parameter to explore a large number of possible solutions, that is about 2.3 million of solutions. For the goodness of fit of the best-fit solution, the misfit between the observed (obs_i) and model-predicted ($pred_i$) displacement is estimated with the reduced chi-square (χ^2), defined as:

$$\chi^2 = \frac{1}{N-m} \sum_{i=1,N} \left(\frac{\text{obs}_i - \text{pred}_i}{\sigma_i} \right)^2 \tag{4}$$

with N is the number of observations, m is the number of model parameters, and σ_i is the uncertainties (4.2 mm here).

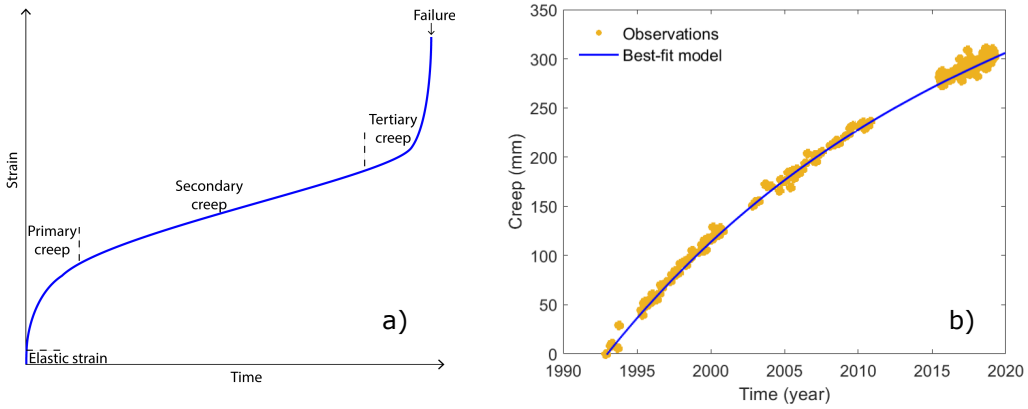

Figure 5. (a) Strain-time plot for a conventional creep experiment. On this typical creep curve, the three creep phases (primary, secondary, and tertiary) are labelled. (b) Time series of the measured displacement and the best fit numerical solution using the extended viscoelastic Burger's model. The model adjusts the data with $\chi^2 = 0.18957$. **Note that to better compare the airport platform deformation to the conventional creep curve, we took the absolute values of the ground displacements.**

Figure 5b shows the best fit numerical solution to the measured displacement over time. The model provides a satisfying fit of observations and adjusts the data with a reduced chi-square of 0.18957, and leads to $\sigma_0 = 0.099$ MPa, $E_M = 32.1$ MPa, $E_{K_1} = 0.86$ MPa, $E_{K_2} = 0.47$ MPa, $\eta_M = 42.63$ MPa/yr, $\eta_{K_1} = 16.21$ MPa/yr, $\eta_{K_2} = 9.61$ MPa/yr. These values are consistent with the range of values obtained in laboratory experiments conducted on clays under triaxial compression condition (Xue et al., 2020). The difference between the observed and modeled displacements reflects mostly the data dispersion as we find a very similar standard deviation, 4.1 mm, for the residues (data minus model). Thus, this result suggests that a transient creep mechanism properly models our observations of the vertical displacement associated with a long-term compaction of materials. Based on this assumption, the airport deformation is still in primary stage of the creep process.

Although the data are well reproduced with an extended Burger's creep model, which allows to investigate a transient rheology for viscous compaction, an extension to a creep damage model in a three-dimensional stress state would be adapted to explore the full non-linear visco-elasto-plastic behavior with potential damage accumulation and accelerated creep (tertiary creep stage in Figure 3d) toward dramatic failure. However, the 1D viscoelastic creep model used here is well adapted to explain the data with a satisfying fit over the 28 years of observation.

5 Discussion and Conclusion

Land use is particularly disputed in coastal areas as they are often highly populated. The intense human activities lead to an increase of various hazards of which vertical land motions due to superficial soil compaction. This latest phenomena can be caused either by natural or anthropogenic phenomena and can lead to further coast erosion, flooding or land salinization in case of ground water pumping. Actually, most of subsidence affecting the costline near big cities are related to ground water

pumping (especially in south-east Asia, like in Jakarta for example), but subsidence is a natural common feature of large river deltas (Nil, Missipi, or Po rivers, for instance) and are due to compaction of the Holocene sediment strata. In the Var river delta (french Riviera, France), we observe the interaction between the natural compaction of the unconsolidated Holocene sediments in the Var river delta with the construction of a man-made infrastructure (the NCA airport) that brought an additional superficial load on top of the sediment. This extra-load leads to amplify drastically the subsidence rate as observed in Cavalié et al. (2015). In the case of the Var river delta, hazard is also amplified by the fact that the overload of sediment has been used to reclaimed land over sea in a place where the continental shelf is narrow and the undersea topography quickly drops to -2500 m (Figure 1). Understanding the mechanism and thus the evolution of sediment compaction is essential to evaluate the danger caused by the coastal subsidence.

Therefore, we use SAR interferometry to measure and analyze the temporal evolution of the ground displacement on the Nice Côte d'Azur airport platform over a long period of 28 years. Extending the observation window to study the long-term subsidence leads to substantial improvements in the understanding of the ongoing mechanisms along this coastal area. Indeed, the previous study (Cavalié et al., 2015) measured the airport platform subsidence using only the Envisat data that span the 2003-2011 period. This relative short period of observation impeded to detect accurately non-linearity of the surface displacement and its change rate. By adding the ERS and Sentinel-1 data, the observation window more than tripled (1992-2020) and times series of the surface displacement clearly reveal a transient non-linear deformation with decelerating subsidence rate over time, that is expected for ground layer compaction. Then, we used a simple analytical Burger's creep model to constrain the mechanisms and rheology at play. The data are properly explained by the primary and secondary creep phases, highlighting a slow viscoelastic deformation at multiyear timescales. The best-fit solution allows to retrieve reasonable mechanical values of the airport sediments that have been brought to build the platform extension. Our study thus proves that the long-term InSAR data can improve our understanding of the surface processes and the subsurface material properties.

Although the subsidence rate decelerates, at least, for 28 years, our results show that the compaction of the sediment is still active and its future evolution is uncertain and still at stake. Indeed, if compaction bands are developing under the airport platform, creep process could potentially lead to accumulated material damage toward failure. Thus, through our investigations, the data indicates that the stability of the airport platform should be monitored continuously with additional high-quality space and land observations together with submarine instrumentation on the continental slope right below the airport. **Indeed, the anticipation of potential future slope failures is a challenging question, especially with the current available data and without understanding the sensitivity of creeping rates in the sediments. The clay sediments can creep at varying rates due to different stressing factors, such as airport platform loading and potential fluid pressure increases from precipitation. Earthquake shaking in this seismic area could also accelerate creep rates. When subjected to high deviatoric load, significant creep may occur, leading to a decrease in sediment resistance and potential slope failure. Moreover, an increase in fluid pressure can reduce effective stress and expedite sediment creeping towards slope failure. Presently, it is clear that the airport platform is slowly creeping, and multiple triggering processes are possible. To gain a comprehensive understanding of the creep characteristics of clay sediments, conducting controlled laboratory experiments under varying disturbance amplitudes and frequencies would be highly beneficial. These experiments**

would allow us to examine the specific influence of different factors on the creep deformation at each stage of the process. Finally, even if the airport platform were absent, the slope would likely still experience creep due to the clay layer, although at a much slower rate and different evolutionary stage. To gain a clearer understanding of the slope's stability under slow, long-term, and fast, dynamic loading, it would be beneficial to gather high-resolution geotechnical, hydrogeological, and seismic data across the Var river delta platform and slope. Combined with geomechanical modeling, such data could help validate the assumptions regarding the slope's stability and provide valuable insights into potential future slope failure scenarios.

In an era in which climate change and sea-level rise pose unprecedented threats to coastal ecosystems and urbanizations (Shirzaei and Bürgmann, 2018; Shirzaei et al., 2021), the long-term observations of ground motions from space is essential to monitor the stability of coastal environment and will inform managers and policymakers identify zones with exposure to hazards.

Data availability. Raw data used in this study are freely available online. Sentinel-1 SAR images are from the PEPS platform (https://peps.cnes.fr/rocket/#/search). ERS and Envisat SAR data were obtained free of charges through a ESA cat1 project (https://earth.esa.int/eogateway/catalog/ers-1-2-sar-im-l0-sar_im__0p- and https://earth.esa.int/eogateway/catalog/envisat-asar-im-l0-asa_im__0p-?text=envisat%20asar%20im%20l0%20%5Basa_im__0p%5D, respecively). The digital elevation model is freely available from JAXA (https://www.eorc.jaxa.jp/ALOS/en/-dataset/aw3d30/aw3d30_e.htm). ERA-5 global reanalyses of atmospheric data are distributed by the ECMWF (https://www.ecmwf.int/en/forecasts/datasets/reanalysis-datasets/era5). Velocity maps shown in Figure 3 are archived on Zenodo (https://doi.org/10.5281/zenodo.7038263).

Author contributions. OC initiated the project and processed the InSAR data with BPP's help. FC analysed the deformation in term of mechanical process and modelled the InSAR data. Everybody got involved in the writing process of the article.

Competing interests. No competing interests are present

Acknowledgements. This work was supported by CNES, focused on data provided by the European space agency (ERS, Envisat and Sentinel-1 missions). We thank the three anonymous reviewers and the editor for their careful reading and comments that improved the original version of the manuscript.

References

Aimaiti, Y., Yamazaki, F., and Liu, W.: Multi-Sensor InSAR Analysis of Progressive Land Subsidence over the Coastal City of Urayasu, Japan, Remote Sensing, 10, https://www.mdpi.com/2072-4292/10/8/1304, 2018.

Ansari, H., De Zan, F., and Parizzi, A.: Study of Systematic Bias in Measuring Surface Deformation With SAR Interferometry, IEEE Transactions on Geoscience and Remote Sensing, 59, 1285–1301, https://doi.org/10.1109/TGRS.2020.3003421, 2021.

Atwater, B. F.: Evidence for great Holocene earthquakes along the outer coast of Washington State, Science, 236, 942–944, 1987.

Berardino, P., Fornaro, G., Lanari, R., and Sansosti, E.: A new algorithm for surface deformation monitoring based on small baseline differential SAR interferograms, IEEE Transactions on Geoscience and Remote Sensing, 40, 2375–2383, https://doi.org/10.1109/TGRS.2002.803792, 2002.

Bland, D. R.: The Theory of Linear Viscoelasticity, New York: Pergamon Press, 1960.

Bürgmann, R., Rosen, P. A., and Fielding, E. J.: Synthetic Aperture Radar interferometry to measure Earth's surface topography and its deformation, Annu. Rev. Earth. Planet. Sci., 28, 169–209, 2000.

Cahoon, D. R., Reed, D. J., and Day Jr, J. W.: Estimating shallow subsidence in microtidal salt marshes of the southeastern United States: Kaye and Barghoorn revisited, Marine geology, 128, 1–9, 1995.

Cavalié, O. and Trouvé, E., eds.: Surface Displacement Measurement from Remote Sensing Images, ISTE - Wiley, 2022.

Cavalié, O., Sladen, A., and Kelner, M.: Detailed quantification of delta subsidence, compaction and interaction with man-made structures : the case of the NCA airport, France, Nat. Hazards Earth Syst. Sci., 15, 1–12, https://doi.org/10.5194/nhess- 15-1-2015, 2015.

Courboulex, F., Mercerat, E. D., Deschamps, A., Migeon, S., Baques, M., Larroque, C., Rivet, D., and Hello, Y.: Strong Site Effect Revealed by a New Broadband Seismometer on the Continental Shelf Offshore Nice Airport (Southeastern France), Pure and Applied Geophysics, 177, 3205–3224, https://doi.org/10.1007/s00024-019-02408-9, 2020.

Dan, G., Sultan, N., , and Savoye, B.: The 1979 Nice harbour catastrophe revisited: Trigger mechanism inferred from geotechnical measurements and numerical modelling, Mar. Geol., 245, 40–64, 2007.

de la Tullaye , M.: Nice-Côte d'Azur, un aéroport gagné sur la mer, Revue XYZ, 38, 43–45, 1989.

De Zan, F., Zonno, M., and López-Dekker, P.: Phase Inconsistencies and Multiple Scattering in SAR Interferometry, IEEE Transactions on Geoscience and Remote Sensing, 53, 6608–6616, https://doi.org/10.1109/TGRS.2015.2444431, 2015.

Doin, M.-P., Lodge, F., Guillaso, S., Jolivet, R., Lasserre, C., Ducret, G., Grandin, R., Pathier, E., and Pinel, V.: Presentation of the small baseline NSBAS processing chain on a case example: the Etna deformation monitoring from 2003 to 2010 using Envisat data, Proc. of FRINGE 2011 Workshop, Frascati, Italy, 19-23 September 2011 (ESA, SP-697, January 2012), 2012.

Du, M., Fouché, O., Zavattero, E., Ma, Q., Delestre, O., and Gourbesville, P.: Water planning in a mixed land use Mediterranean area: point-source abstraction and pollution scenarios by a numerical model of varying stream-aquifer regime, Environmental Science and Pollution Research, 26, 2145–2166, https://doi.org/10.1007/s11356-018-1437-0, 2019.

Farrell, W. and Clark, J.: On Postglacial Sea Level, Geophys. JR Astron. Soc., 46, 647–667, 1976.

Fattahi, H. and Amelung, F.: InSAR bias and uncertainty due to the systematic and stochastic tropospheric delay, Journal of Geophysical Research: Solid Earth, 120, 8758–8773, https://doi.org/10.1002/2015JB012419, 2015.

Findley, W. N., Lai, J. S., and Onaran, K.: Creep and Relaxation of Nonlinear Viscoelastic Materials, New York: North-Holland Publishing Company, 1976.

Frederikse, T., Landerer, F., Caron, L., Adhikari, S., Parkes, D., Humphrey, V. W., Dangendorf, S., Hogarth, P., Zanna, L., Cheng, L., et al.: The causes of sea-level rise since 1900, Nature, 584, 393–397, 2020.

Galloway, D. L. and Burbey, T. J.: Regional land subsidence accompanying groundwater extraction, Hydrogeology Journal, 19, 1459–1486, 2011.

Grandin, R., Doin, M.-P., Bollinger, L., Pinel-Puysségur, B., Ducret, G., Jolivet, R., and Sapkota, S. N.: Long-term growth of the Himalaya inferred from interseismic InSAR measurement, Geology, 40, 1059–1062, https://doi.org/10.1130/G33154.1, 2012.

Jaeger, J. C. and Cook, N. G.: Fundamentals of Rock Mechanics, Chapman and Hall, London, U.K, 1979.

Jiang, Z. and Wang, H.: Study on Shear Creep Characteristics and Creep Model of Soil-Rock Mixture Considering the Influence of Water Content, Frontiers in Physics, 10, https://doi.org/10.3389/fphy.2022.819709, 2022.

Kendall, R. A., Mitrovica, J. X., and Milne, G. A.: On post-glacial sea level–II. Numerical formulation and comparative results on spherically symmetric models, Geophysical Journal International, 161, 679–706, 2005.

Kopf, A. J., Stegmann, S., Garziglia, S., Henry, P., Dennielou, B., Haas, S., and Weber, K.-C.: Soft sediment deformation in the shallow submarine slope off Nice (France) as a result of a variably charged Pliocene aquifer and mass wasting processes, Sedimentary Geology, 344, 290–309, https://doi.org/https://doi.org/10.1016/j.sedgeo.2016.05.014, 2016.

Leynaud, D. and Sultan, N.: 3-D slope stability analysis: A probability approach applied to the nice slope (SE France), Mar. Geol., 269, 89–106, 2010.

Li, G., Zhao, C., Wang, B., Liu, X., and Chen, H.: Land Subsidence Monitoring and Dynamic Prediction of Reclaimed Islands with Multi-Temporal InSAR Techniques in Xiamen and Zhangzhou Cities, China, Remote Sensing, 14, https://www.mdpi.com/2072-4292/14/12/2930, 2022.

Liao, M., Cui, D., Bao, X., Qiao, Z., and Zhao, C.: Creep Characteristics of Soil in the Sliding Zone of Huangtupo Landslide, Applied Sciences, 12, https://doi.org/10.3390/app122312439, 2022.

Métois, M., Benjelloun, M., Lasserre, C., Grandin, R., Barrier, L., Dushi, E., and Koçi, R.: Subsidence associated with oil extraction, measured from time series analysis of Sentinel-1 data: case study of the Patos-Marinza oil field, Albania, Solid Earth, 11, 363–378, 2020.

Milliman, J. D. and Haq, B. U.: Sea-level rise and coastal subsidence: Causes, consequences, and strategies, vol. 2, Springer Science & Business Media, 1996.

Ollié, J.-P.: L'extension sud de l'aéroport international de Nice - Côte d'Azur. Le point sur les travaux, Revue générale des routes et des aérodromes, 1982.

Oppenheimer, M., Glavovic, B. C., Hinkel, J., van de Wal, R., Magnan, A. K., Abd-Elgawad, A., Cai, R., Cifuentes-Jara, M., DeConto, R. M., Ghosh, T., Hay, J., Isla, F., Marzeion, B., Meyssignac, B., and Sebesvari, Z.: 2019: Sea Level Rise and Implications for Low-Lying Islands, Coasts and Communities, In: IPCC Special Report on the Ocean and Cryosphere in a Changing Climate [H.-O. Pörtner, D.C. Roberts, V. Masson-Delmotte, P. Zhai, M. Tignor, E. Poloczanska, K. Mintenbeck, A. Alegría, M. Nicolai, A. Okem, J. Petzold, B. Rama, N.M. Weyer (eds.)]., 2019.

Park, S.-W. and Hong, S.-H.: Nonlinear Modeling of Subsidence From a Decade of InSAR Time Series, Geophysical Research Letters, 48, e2020GL090 970, https://doi.org/10.1029/2020GL090970, e2020GL090970 2020GL090970, 2021.

Peltier, W. R.: Global glacial isostasy and the surface of the ice-age Earth: the ICE-5G (VM2) model and GRACE, Annu. Rev. Earth Planet. Sci, 32, 2004.

Pinel-Puysségur, B., Michel, R., and Avouac, J.-P.: Multi-Link InSAR Time Series: Enhancement of a Wrapped Interferometric Database, IEEE Journal of Selected Topics in Applied Earth Observations and Remote Sensing, 5, 784–794, https://doi.org/10.1109/JSTARS.2012.2196758, 2012.

Plant, G. W., Covil, C. S., and Hughes, R. A.: Site preparation for the new Hong Kong International Airport, Thomas Telford Publishing, https://doi.org/10.1680/spftnhkia.26964, 1998.

Rohmer, O., Bertrand, E., Mercerat, E., Régnier, J., Pernoud, M., Langlaude, P., and Alvarez, M.: Combining borehole log-stratigraphies and ambient vibration data to build a 3D Model of the Lower Var Valley, Nice (France), Engineering Geology, 270, 105 588, https://doi.org/https://doi.org/10.1016/j.enggeo.2020.105588, 2020.

Schaeffer, M., Hare, W., Rahmstorf, S., and Vermeer, M.: Long-term sea-level rise implied by 1.5 °C and 2 °C warming levels, Nature Climate Change, 2, 867–870, https://doi.org/10.1038/nclimate1584, 2012.

Shirzaei, M. and Bürgmann, R.: Global climate change and local land subsidence exacerbate inundation risk to the San Francisco Bay Area, Science Advances, 4, https://doi.org/10.1126/sciadv.aap9234, 2018.

Shirzaei, M., Freymueller, J., Törnqvist, T. E., Galloway, D. L., Dura, T., and Minderhoud, P. S. J.: Measuring, modelling and projecting coastal land subsidence, Nature Reviews Earth & Environment, 2, 40–58, https://doi.org/10.1038/s43017-020-00115-x, 2021.

Stegmann, S., Sultan, N., Kopf, A., Apprioual, R., and Pelleau, P.: Hydrogeology and its effect on slope stability along the coastal aquifer of Nice, France, Marine Geology, 280, 168–181, 2011.

Sudhaus, H. and Sigurjón, J.: Improved source modelling through combined use of InSAR and GPS under consideration of correlated data errors: application to the June 2000 Kleifarvatn earthquake, Iceland, Geophys. J. Int., 176, 389–404, https://doi.org/10.1111/j.1365-246X.2008.03989.x, 2009.

Sultan, N., Garziglia, S., Bompais, X., Woerther, P., Witt, C., Kopf, A., and Migeon, S.: Transient Groundwater Flow Through a Coastal Confined Aquifer and Its Impact on Nearshore Submarine Slope Instability, Journal of Geophysical Research: Earth Surface, 125, https://doi.org/https://doi.org/10.1029/2020JF005654, 2020.

Sun, T. and Wang, K.: Viscoelastic relaxation following subduction earthquakes and its effects on afterslip determination, J. Geophys. Res., 120, 1329–1344, https://doi.org/10.1002/2014JB011707, 2015.

Wigley, T. M. L. and Raper, S. C. B.: Thermal expansion of sea water associated with global warming, Nature, 330, 127–131, https://doi.org/10.1038/330127a0, 1987.

Wöppelmann, G. and Marcos, M.: Vertical land motion as a key to understanding sea level change and variability, Reviews of Geophysics, 54, 64–92, https://doi.org/10.1002/2015RG000502, 2016.

Wu, P.-C., Wei, M., and D'Hondt, S.: Subsidence in Coastal Cities Throughout the World Observed by InSAR, Geophysical Research Letters, 49, https://doi.org/10.1029/2022GL098477, 2022.

Wu, S., Yang, Z., Ding, X., Zhang, B., Zhang, L., and Lu, Z.: Two decades of settlement of Hong Kong International Airport measured with multi-temporal InSAR, Remote Sensing of Environment, 248, 111 976, https://doi.org/https://doi.org/10.1016/j.rse.2020.111976, 2020.

Xiong, Z., Deng, K., Feng, G., Miao, L., Li, K., He, C., and He, Y.: Settlement Prediction of Reclaimed Coastal Airports with InSAR Observation: A Case Study of the Xiamen Xiang'an International Airport, China, Remote Sensing, 14, https://www.mdpi.com/2072-4292/14/13/3081, 2022.

Xue, K., Wang, S., Hu, Y., and Li, M.: Creep Behavior of Red-Clay Under Triaxial Compression Condition, Frontiers in Earth Science, 7, https://doi.org/10.3389/feart.2019.00345, 2020.

Yao, Y., Cheng, H., Lin, J., and Ji, J.: Optimization of Burgers creep damage model of frozen silty clay based on fuzzy random particle swarm algorithm, Scientific Reports, 11, 18 974, https://doi.org/10.1038/s41598-021-98374-1, 2021.

Zou, L., Wang, S., and Lai, X.: Creep model for unsaturated soils in sliding zone of Qianjiangping landslide, Journal of Rock Mechanics and Geotechnical Engineering, 5, 162–167, https://doi.org/10.1016/j.jrmge.2013.03.001, 2013.